UC San Diego

UC San Diego Previously Published Works

Title

Statistical damage detection based on full-field covariance of circumferential scan ultrasonic measurement

Permalink

https://escholarship.org/uc/item/7t90d4wq

Authors

Chong, See Yenn
Todd, Michael D

Publication Date

2018-03-27

DOI

10.1117/12.2297601

Peer reviewed

eScholarship.org Powered by the California Digital Library
University of California

Statistical damage detection based on full-field covariance of circumferential scan ultrasononic measurement

See Yenn Chong*[a], Michael D Todd[a]
[a]Department of Structural Engineering, University of California, San Diego, 9500 Gilman Dr., La Jolla, CA, USA 92093

ABSTRACT

Laser ultrasonic techniques (LUTs) perform an inspection based on raster scanning pattern to obtain three-dimensional (3D) ultrasonic signals for damage detection in mechanical structures. Even though the raster scan-based in LUTs provides full-field ultrasonic data with high spatial resolution, the scan process consumes substantial time and generates redundant ultrasonic data in many applications.. In this paper, statistical damage detection based on the full-field covariance of circumferential scanning is proposed to accelerate the damage detection process using LUTs. A laser ultrasonic interrogation method based on a Q-switched laser scanning system was used to interrogate 3D ultrasonic signals in a 6-mm aluminum plate with four square through-thickness at four different depths. The circumferential scans at a given radius were obtained from the 3D ultrasonic wavefield and represented in a two-dimensional (2D) matrix, angle-time (θ-t) domain. The proposed method was tested at three different circumferences where the defects were located right on, outside, and inside the area of the scan circumference. The covariance matrix, $\mathbf{C}_\theta$, of the vector variables in θ-direction was calculated and represented as a covariance image. The covariance image of $\mathbf{C}_\theta$ demonstrated the ability to detect the defects at these three different circumferences. Hence, the covariance map of an ultrasound circumference can facilitate the existing LUTs to determine the damage existence instead operate in raster scanning mode.

Keywords: Non-destructive evaluation, full-field ultrasonic inspection, covariance matrix, laser ultrasonic techniques

1. INTRODUCTION

Laser ultrasonic techniques (LUTs) have been intensively developed for NDE and SHM applications, owing to their non-contact nature and high spatial resolution. Additionally, full-field ultrasonic data may be formed in a 3D space-time volume and intuitively interpreted without prior in-depth knowledge of the wavefield. LUTs are also showed the applicability to both isotropic metals and anisotropic composite materials [1-5].

Nonetheless, LUTs have significant challenges in practical implementation [6]. One of the challenges is slow data acquisition. Even though the LUTs have the capability to perform a large-scale structure inspection with high spatial resolution of full-field ultrasonic data, it may be impractical to perform the inspection when there is no information about the damage existence, especially for periodic maintenance service. Commonly, raster scan pattern is employed in LUTs to generate ultrasonic wavefield in Cartesian coordinate space because it has better local damage detection. However, raster-scanning time is proportional to the required inspection area. In addition, the scanning process can take significant time as well when a laser repeat scanning process is employed to overcome the poor signal-to-noise ratios of the full-field ultrasonic data, especially when laser Doppler vibrometry is used as part of the acquisition [7].

Recently, several methods are introduced to improve the speed of full-field ultrasonic data acquisition. For the laser ultrasonic generator-based system, the Q-switched laser scanning system with 20-kHz scanning speed showed the feasibility of damage detection on a CFRP plate [8]. This has significantly improved the speed of the full-field ultrasonic data acquisition; e.g. it takes only 2 seconds to complete a scan area of 100 mm × 100 mm at 0.5 mm scan interval. The Q-switched laser scanning system is configured to synchronize with a data acquisition (DAQ) module by periodically triggering the DAQ to acquire a local ultrasonic signal. The period of this triggering signal is based on the scanning speed, so the maximum length of an acquired ultrasound at each scan point is limited by the scanning speed. In this case,

* Corresponding author. Email: s3chong@eng.ucsd.edu; phone 1 858 534-5993

the maximum length of an acquired ultrasound is only 50 μs at the scanning speed of 20 kHz. In addition, the high laser scanning speed is not suitable for metallic structure inspection where the reverberative field has a long dwell time.

Compressed sensing (CS) technique has recently emerged as a novel signal acquisition paradigm that enables the reconstruction of high-dimensional signals with relatively few measurements. This technique has grasped the attention of researchers in NDE and SHM communities and introduced to expedite the acquisition process in ultrasonic wavefield data [9-12]. Di Ianni et al. [10] demonstrated that the signal decomposition based on the Fourier domain has better recovery accuracy with less than 34% of the original sampling grid. Mesnil and Ruzzene [11] showed also the ability of CS technique for damage detection with a significantly reduced number of measurements. Harley and Chia [13] introduced a framework to use sparse wavenumber analysis based on CS [14] to create a damage-free model of the wavefield. Then, this model was combined with matched field processing to image damage from a small number of partial wavefield measurements. As the results, these methods improved the scan time of current wavefield imaging. On the other hand, Park et al. [12] proposed an accelerated laser scanning technique based on binary search and compressed sensing to localize and visualize damage with reduced scanning points and scanning time. The number of scanning points in the composite plate experiment is reduced by 97.1% (from 2601 points to 75 points). In CS technique, the dictionary signal is used to reconstruct the high-resolution signal. Thus, the performance of the signal reconstruction is dependent on dictionary quality. Consequently, long post-processing time and high computational burden may be needed to obtain the "best" dictionary through a dictionary learning algorithm [15].

In general, the damage diagnosis strategy involves the processes of detection, localization, and evaluation, especially for SHM implementation. In a diagnosis strategy, damage *detection* is always the initial process to detect the anomalies in structures, followed by localization and then characterization (size, type, etc.) . In general, the existing LUTs conduct the inspection process by directly performing the raster scanning without knowing either damage exists or not. Thus, to avoid this LUTs performing the inspection "blindly", it is necessary to incorporate a detection algorithm into the laser scanning system. In this paper, a covariance method for circumference ultrasound is proposed to accomplish this to facilitate the existing LUTs to perform the large-scale inspection with substantive time-cost reduction. The following sections of this paper will present the experimental setup for obtaining the full-field ultrasonic data using laser ultrasonic interrogation system (LUIS), the theory and implementation of the covariance matrix for the circumferential ultrasound, and the results discussion.

2. EXPERIMENTAL SETUP

Figure 1(a) shows a schematic diagram of a laser ultrasonic interrogation system. This system consists of a laser scanning system incorporated with a signal conditioning device, a data acquisition (DAQ) module, a contact sensor, and a computer used for signal processing and operation control. The laser scanning system has a two-dimensional laser scanner and a diode-pumped solid-state Q-switched Nd:YAG laser. The Q-switched laser is composed of a laser controller and a laser head with output beam of 527 nm wavelength and pulse repetition rates (PRR) from single-shot to 1 kHz. The 2D laser scanner is used to synchronize the 2-axis galvanometer scanner (Fig. 1(a)) with the Q-switched laser to maneuver the laser impinging point rapidly on a target at a PRR to perform a raster scanning process.

In the scanning process, a laser pulse impinges at a scan point, and the corresponding ultrasound is generated at the local point based on the thermoelastic principle. The generated ultrasound is then signal-conditioned through a contact sensor and digitized in the DAQ module as shown in Fig. 1(a). In the DAQ module, the generated ultrasound is digitized synchronously with the PRR of the laser scanning system by receiving a triggering signal from the laser controller after the laser pulse is emitted. In the digitizing process, the ultrasound is sampled for K number of data points at sampling time interval T_S and stored in a computer. The digitizing process is repeated as the scanning process is performed. Once the scanning process is completed, the ultrasound in 2D space with X and Y grid of points on the target are generated and all generated ultrasonics are generated in the form of a three-dimensional X by Y by T matrix, indexed by spatial-x-direction, spatial-y-direction, and k time samples, respectively, along with each dimension.

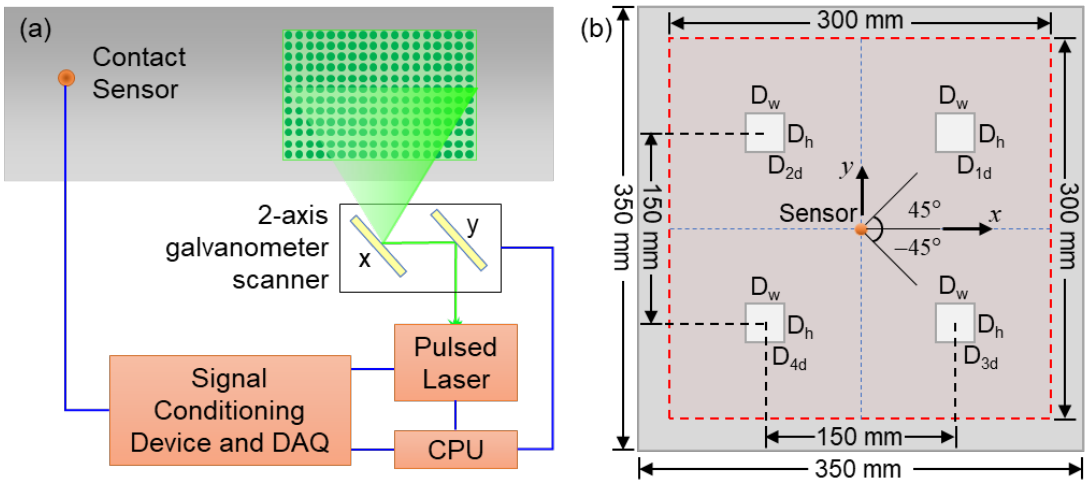

Figure 1. (a) Laser ultrasonic interrogation system configuration and (b) a 6-mm aluminum plate with four square through-thickness defects.

Figure 1(b) shows a 6-mm thick aluminum plate with four square through-thickness defects. These square through-thickness were made with the dimension size of 30 mm (D_h) × 30 mm (D_w) and the depths were 5 mm (D_{1d}), 4 mm (D_{2d}), 3 mm (D_{3d}), and 1.5 mm (D_{1d}) respectively. The angle directions of these defects from the center point (a sensor point) were ±45° and ±135° as shown in Fig. 1(b). To reduce the reverberation effects in an aluminum plate, the PRR of the laser scanning system was set at 20 Hz with the pulsed energy of 1 mJ (fluence of 23 mJ/cm^2). The aluminum plate was set up at a stand-of-distance of 1770 mm from the 2D laser scanner and the area of interest was 300 mm × 300 mm with a scan interval of 0.5 mm. An ultrasonic sensor bonded at the center of the rear scanning surface of the aluminum plate. An in-line bandpass filter was used in this research to filter ultrasonic signals at the frequency range of 100 kHz to 300 kHz. The ultrasonic signal was sampled by the DAQ module with a sampling time of T_S = 0.2 μs and K = 1000 total sample points. Lastly, the ultrasonic wavefield imaging (UWI) was generated based on this 3D ultrasonic data in the computer.

3. COVARIANCE MATRIX OF CIRCUMFERENTIAL ULTRASOUNDS

3.1 Ultrasonic wavefield imaging

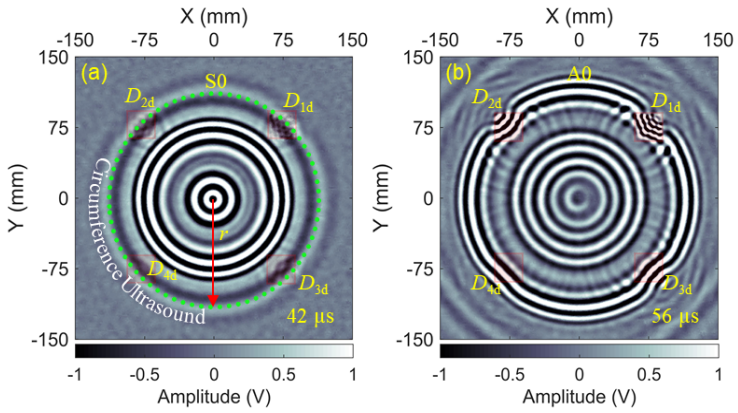

Figure 2. Ultrasonic wavefield image at the time-frame of (a) 42 μs and (b) 56 μs.

Figure 2 shows the ultrasonic wavefield imaging generated at the different time-frame. Since the ultrasonic wavefield propagation imaging is generated based on the reciprocity of ultrasonic propagation [16], the wavefield imaging as shown in Fig. 2 shows that the ultrasonic waves emitted from the sensor point (0, 0). Commonly, the incident waves of the ultrasound propagating in a pristine aluminum plate (isotropic material) are the same along the circumference.

However, as shown in Figs. 2(a) and (b), the local incident waves were distorted at the damaged areas (D_{1d} - D_{4d}) as compared to the incident waves in the pristine areas. It is a hypothesis that a local damage may be identified by correlating the local distorted waves with the adjacent waves in the pristine area through a spatial covariance.

3.2 Circumferential ultrasounds

The scope of this paper is to study the feasibility of the proposed method using circumferential wave propagation similarity for damage detection. Hence, in this paper, the implementation of the circle scan in the LUIS to obtain the circumference ultrasounds was not considered.

The circumferential ultrasounds at a fixed radius r from a source point can be obtained from the 3D ultrasound data generated by the LUIS. In the scanning processing (Fig. 1(a)), ultrasonic data are generated at the scan points based on Cartesian coordinate scheme. So, the circumferential ultrasounds at the radius of r in the polar coordinate are obtained with the following expressions:

$$r = \sqrt{x^2 + y^2} \text{ and } \theta = \tan^{-1}(x, y) \tag{1}$$

where x and y are the samples of the 2-D spatial domain and θ is the circumferential angles from −180° to 180°. The sensor located on the aluminum plate (Fig. 1(b)) was set as the central point of the circle. With the Eqn. (1), the circumferential ultrasounds at a fixed r are determined for all angles θ. Then, these ultrasounds are plotted in the angle-time domain as shown in Fig. 4. The circumferential ultrasound image is formed in $N \times K$ matrix. The index n is assigned as a number to each angle sample, ranging from 1 to N; and the index k is assigned as the number to each time sample, ranging from 1 to K.

The damage may be generated at any location with no prior knowledge of an inspection target. Hence, to test the detectability of the covariance method, the ultrasounds at the three different circumferences were considered in this paper as shown in Fig. 3. Two circumferences at the radii of 75 mm and 125 mm were selected for the cases where the damage is located outside and inside the area of the circumference. The other one is at the radius of 100 mm for the case that the damage is located right on the circumference.

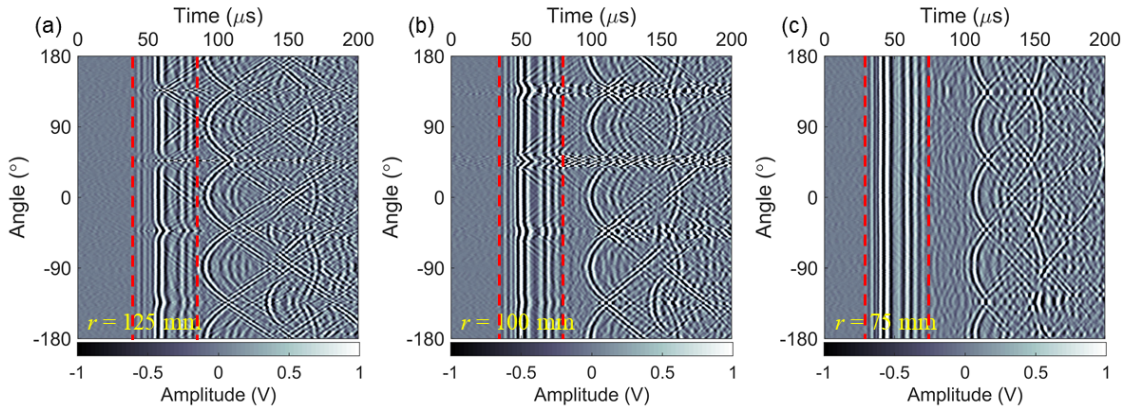

Figure 3. Circumferential ultrasounds obtained at the radii of (a) 125 mm, (b) 100 mm, and (c) 75 mm.

3.3 Covariance of circumferential ultrasound

Covariance is principally used to learn the correlation structure among the variable vectors of a data set. As used here, it reveals the characteristics of the spatial correlation among the local waves at each instant in time. Thus, it allows us to determine the correlation of the waves along the same circumference for all the angular directions. With that, the covariance responses may be used to identify the distorted waves that allow us to determine either there is a damage or not in an inspection target.

For that, the covariance matrix of circumferential ultrasounds at a radius r (Fig. 3) is calculated. Since circumferential data are formed in $N \times K$ matrix, the elements of the $N \times K$ matrix are wave amplitudes and grouped into a row vector Θ_n for θ-axis.

For the covariance matrix of Θ_n, the $N \times K$ of the circumferential data (Fig. 3) is transposed first and yielded a column vector $\Theta_n^T = \left\{\theta_{1,n}, \theta_{2,n}, \cdots, \theta_{K,n}\right\}$ with a set of ultrasonic amplitude values (denoted as $\theta_{k,n}$) in temporal samples. The covariance matrix of Θ_n^T is denoted as $\mathbf{C}_\Theta$ and expressed below:

$$\mathbf{C}_\Theta = \begin{pmatrix} c_{1,1} & c_{1,2} & \cdots & c_{1,N} \\ c_{2,1} & c_{2,2} & \cdots & c_{2,N} \\ \vdots & \vdots & \ddots & \vdots \\ c_{N,1} & c_{N,2} & \cdots & c_{N,N} \end{pmatrix}, \tag{2}$$

and the elements of $\mathbf{C}_\Theta$ are defined as:

$$c_{ij} = \frac{1}{K-1}\sum_{k=1}^{K}\left(\theta_{k,i} - \overline{\theta}_i\right)\left(\theta_{k,j} - \overline{\theta}_j\right) \tag{3}$$

where $i, j = 1, 2, \cdots, N$, and $\overline{\theta}_i$ and $\overline{\theta}_j$ are the mean of each column vector Θ_n^T. Since the covariance matrix in Eqn. (2) is a symmetric matrix with the matrix size of $N \times N$, for $i = j$ the diagonal elements, denoted as c_{ii}, contain the variances of column vector Θ_n^T; for $i \neq j$ the off-diagonal elements contain the covariance between all possible pairs of a column vector Θ_n^T. Then, the covariance map of the circumferential data at a fixed radius may be obtained based on Eqn. (2). Next, the covariance map is analyzed to identify the damage.

4. RESULTS AND DISCUSSIONS

In LUIS, the pulsed laser was used to generate ultrasound at each scan points in the 2D spatial domain. Consequently, each scan point on the circumference was treated as a point source, and the ultrasound was generated at the local scan point of the circumference. These generated waves propagated and then were received at the sensor point. Figures 3(a) and (b) show the circumferential ultrasounds at the radii of 125 mm and 100 mm received at the sensor, respectively. At the angle directions of ±45° and ±135°, these waves were distorted as they propagated through the damage regions before they reached the sensor. Since the circumferential ultrasounds generated at the radius of 75 mm were in between the square through-thickness and the sensor point, the sensor received the incident waves first, followed by the reflected waves from the damages boundaries and the plate boundaries. Hence, the incident waves of the circumferential waves at the radius of 75 mm showed no distortion as shown in Fig. 3(c).

Figure 4 shows the covariance maps for the circumferential ultrasounds at the radii of 125 mm, 100 mm, 75 mm. In Fig. 4(a), the covariance map showed the covariance responses of the circumferential ultrasounds at the radius of 125 mm. The covariance map indicated the distinguished black lines (covariance values increased negatively) at the same angles of the damages located. In Fig. 4(b), the covariance map showed the covariance responses of the circumference ultrasounds at the radius of 100 mm. The covariance map indicated that the dark lines were faded when the through-thickness depths were reduced. As the results, it was difficult to detect the damage with the through-thickness depth of 1.5 mm. The observations in Figs. 4(a) and (b) demonstrated that the covariance map was able to detect the damage when it was inside the area of the circumference or on the circumference. For the circumferential waves at the radius of 75 mm, the covariance map (Fig. 4(c)) showed no damage detection since the damage was located outside the area of the circumference.

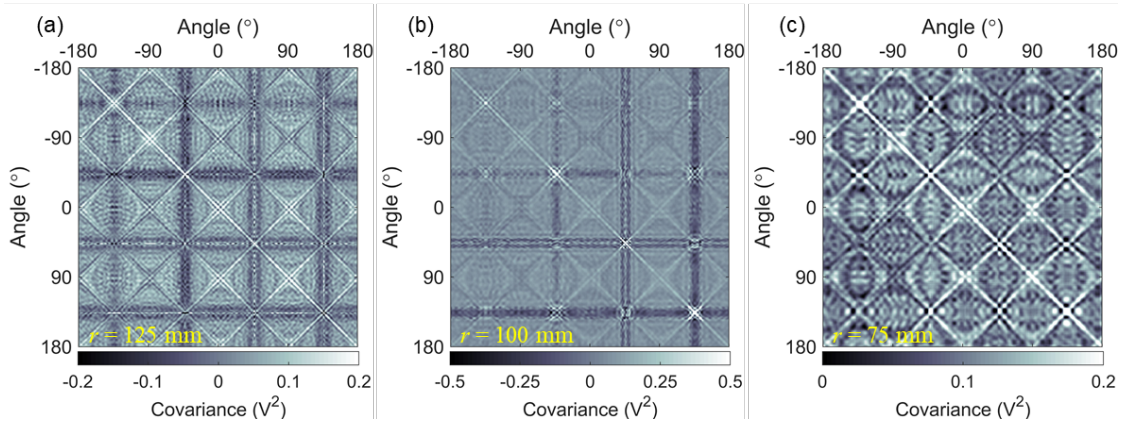

Figure 4. Covariance responses of circumferential ultrasounds obtained at the radii of (a) 125 mm, (b) 100 mm, and (c) 75 mm.

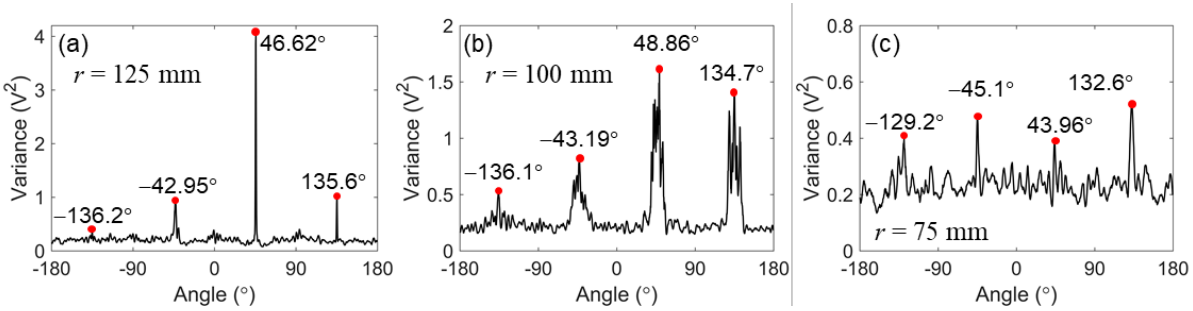

Figure 5. Variance responses of circumferential ultrasounds obtained at the radii of (a) 125 mm, (b) 100 mm, and (c) 75 mm.

In the covariance matrix, the variances (diagonal values) can be used as a feature to detect the damages. These variances of the covariance maps in Figs. 4(a-c) were plotted in Figs. 5(a-c) respectively. For all three cases, the corresponding variances showed high peaks at about the same angle directions of the damages. For the cases of 125 mm and 100 mm, the damages were detected in the covariance map and the variances. For the case of 75 mm, the covariance map was not able to detect the damage (Fig. 4(c)), but the variances showed the ability to detect damages even though the damages were outside the area of the circumference.

In general, the wavefield can be classified into a noise wavefield, an incident wavefield, and a reflected wavefield. These wavefield types can be identified at the different time ranges as shown in Fig. 3. Hence, the covariance responses of these wavefield types may be different from each other. In this paper, each wavefield type was separated manually by selecting a different time range from the circumferential ultrasound image. The red-shaped lines in Fig. 3 showed the selected time ranges for the wavefield classes, respectively. Then, each wavefield type was extracted based on the selected time ranges. After that, the covariance of this extracted wavefield was calculated using Eqn. (2).

Figures 6(a-c) show the covariance maps of the noise wavefield, incident wavefield, and reflected wavefield of the circumferential ultrasounds at the radius of 75 mm respectively. In Figs. 6(a) and (b), no damages were identified in the covariance maps of these two wavefields. Then, the corresponding variances, as shown in Figs. 7(a) and (b), were also showed no strong peaks that in relation to the damages. The covariance responses of the reflected wavefield in Fig. 6(c) showed also no damage detection, same as the case discussed in Fig. 4(c). However, the variances of this reflected wavefield as shown in Fig. 7(c) were able to detect the damages.

In Fig. 6, each covariance map showed the distinctive map pattern of each wavefield type. The covariance map of the reflected wavefield (Fig. 6(c)) showed multiple “diagonal square shapes” and this map was similar to the covariance map in Fig. 4(c). It is likely that the pattern “diagonal square shape” in the covariance map was formed due to the reflected waves from the boundaries of a square plate. Hence, this explains that why the covariance maps in Figs. 4(a) and (b) have the “diagonal square shape” as well. To further verify the claim, the circumference ultrasound at the radii of 125 mm and 100 mm were separated into three wavefields as shown in Figs. 3(a) and (b).

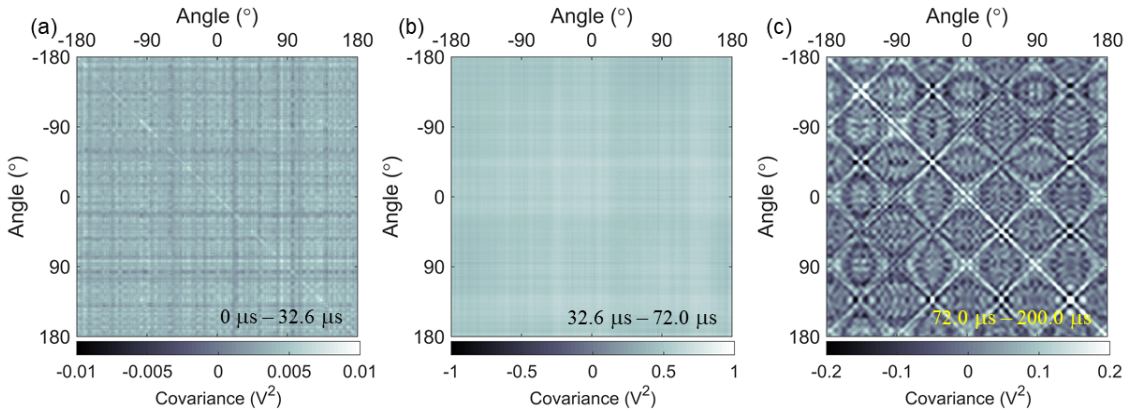

Figure 6. Covariance responses of three different wavefields, (a) noise wavefield, (b) incident wavefield, and (c) reflected wavefield, for a circumferential ultrasound at the radius of 75 mm.

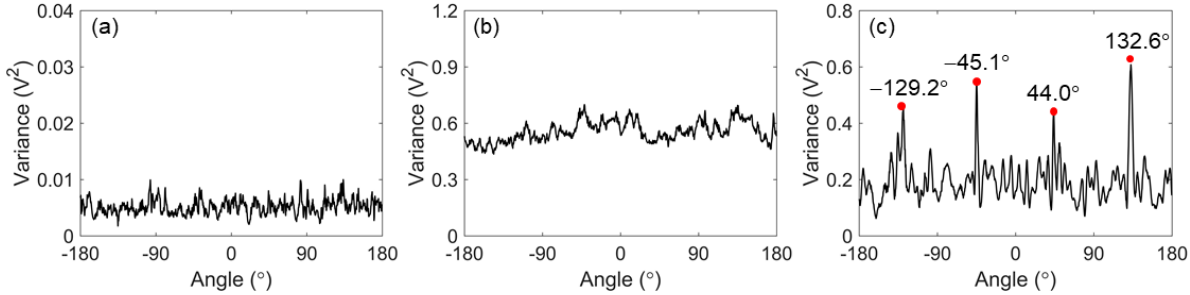

Figure 7. Variance responses of three different wavefields, (a) noise wavefield, (b) incident wavefield, and (c) reflected wavefield, for a circumferential ultrasound at the radius of 75 mm.

Figure 8 shows the covariance responses of the three wavefield types of the circumferential ultrasounds at the radius of 100 mm. The covariance maps of these wavefield types showed the damage. The covariance map in Fig. 8(b) showed that the map was more "clean" as compared to the previous case in Fig. 4(b) since the "diagonal square shape" was not formed. For that, in Figs. 8(a) and (b), the covariance maps have enhanced the detectability of the lowest hole depth (D_{4d}) as compared to the previous case in Fig. 4(b). The covariance map of the reflected wavefield showed the form of the "diagonal square shape" as well and the anomalous lines were observed in the angle directions where the damage was located, as shown in Fig. 8(c). This showed that the covariance map of the reflected wavefield was able to detect the damage too. In addition, the variances for these three wavefield types as shown in Fig. 9 also showed the detection of the damages.

Figure 10 shows the covariance responses of the three wavefield types of the circumferential ultrasounds at the radius of 125 mm. As for the noise wavefield, the covariance and variance marginally detected the damage. Figure 10(b) shows the covariance responses of the incident wavefield were "clean" too. The variances as shown in Fig. 11 also showed the ability to detect the damages. Then, the covariance response of the reflected wave for this ultrasonic signal at the radius of 125 mm showed only marginally detect the damage. Its variances also showed good detection of the damage D_{1d}, D_{2d}, and D_{3d}. But, the damage D_{4d} is marginally identified since the depth is very low as compared to the other depth.

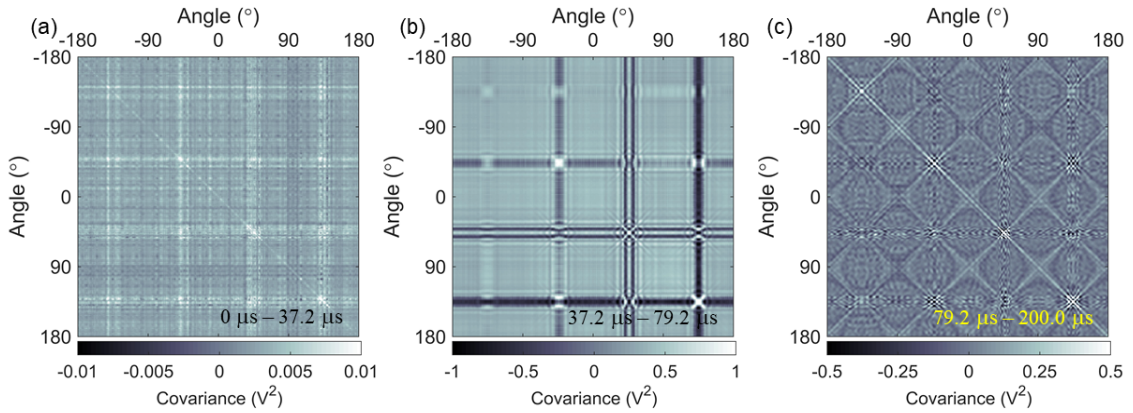

Figure 8. Covariance responses of three different wavefields, (a) noise wavefield, (b) incident wavefield, and (c) reflected wavefield, for a circumferential ultrasound at the radius of 100 mm.

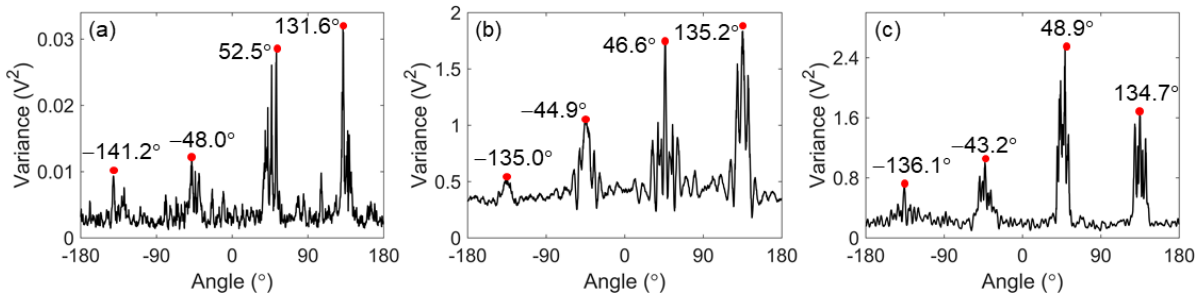

Figure 9. Variance responses of three different wavefields, (a) noise wavefield, (b) incident wavefield, and (c) reflected wavefield, for a circumferential ultrasound at the radius of 100 mm.

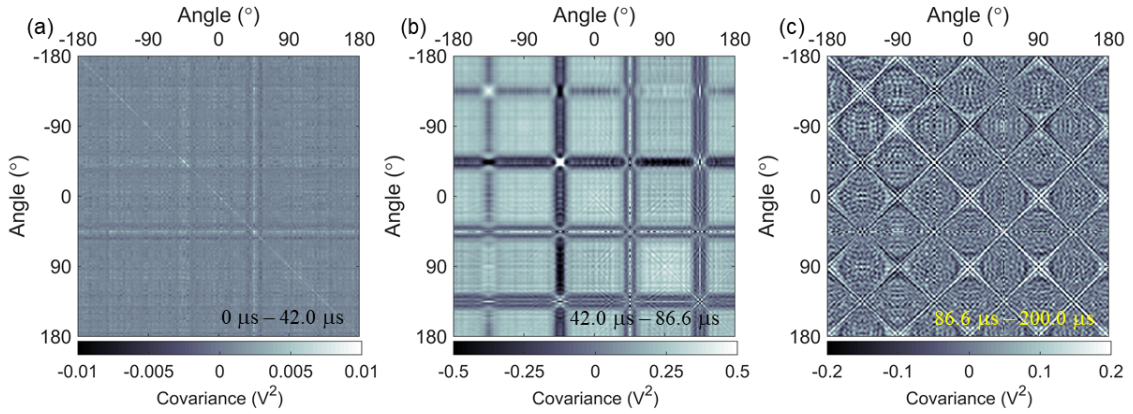

Figure 10. Covariance responses of three different wavefields, (a) noise wavefield, (b) incident wavefield, and (c) reflected wavefield, for a circumferential ultrasound at the radius of 125 mm.

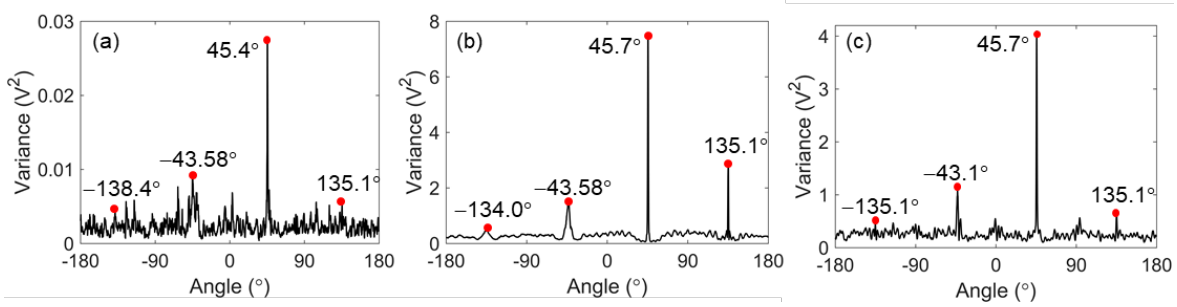

Figure 11. Variance responses of three different wavefields, (a) noise wavefield, (b) incident wavefield, and (c) reflected wavefield, for a circumferential ultrasound at the radius of 125 mm.

5. SUMMARY

This article presents a new approach to damage detection method that may facilitate existing LUTs to perform large-scale inspection in a more efficient way. A spatial covariance method was introduced to analyze the circumferential wavefront. The covariance map demonstrated the ability to detect the damages when the damage was located within the area of the wavefront scan point circumference. However, the damage was not able to be identified when the damage was located outside the area of the circumference. The covariance map of the incident waves showed better visibility to identify the damage at the depth of 1.5 mm. On the other hand, the variances of the covariance maps showed the ability to detect the damage regardless which circumferences were considered. The proposed method demonstrated the ability to detect the damage with the corresponding angle direction from the sensor. However, the damage in 2D space cannot be localized with only the identified angular direction from the proposed method. Hence, to localize the damage in 2D space, the radius from the center point to the damage must be determined as well. For future work, a damage localization method will be developed to estimate the radius at the damage.

REFERENCES

[1] Chong SY, Lee J-R, Chan YP. Statistical threshold determination method through noise map generation for two dimensional amplitude and time-of-flight mapping of guided waves. Journal of Sound and Vibration. 2013;332:1252-64.
[2] Flynn EB, Chong SY, Jarmer GJ, Lee J-R. Structural imaging through local wavenumber estimation of guided waves. Ndt & E International. 2013;59:1-10.
[3] Tian Z, Yu L, Leckey C. Delamination detection and quantification on laminated composite structures with Lamb waves and wavenumber analysis. Journal of Intelligent Material Systems and Structures. 2015;26:1723-38.
[4] Chong SY, Victor JJ, Todd MD. Full-field ultrasonic inspection for a composite sandwich plate skin-core debonding detection using laser-based ultrasonics. SPIE Smart Structures and Materials + Nondestructive Evaluation and Health Monitoring: SPIE; 2017. p. 10.
[5] Byeongjin P, Hoon S. Accelerated damage visualization using binary search with fixed pitch-catch distance laser ultrasonic scanning. Smart Materials and Structures. 2017;26:075005.
[6] Michaels JE. Ultrasonic wavefield imaging: Research tool or emerging NDE method? AIP Conference Proceedings. 2017;1806:020001.
[7] Jung-Ryul L, See Yenn C, Nitam S, Chan Yik P. Repeat scanning technology for laser ultrasonic propagation imaging. Measurement Science and Technology. 2013;24:085201.
[8] Chong S, Lee J. Development of laser ultrasonic propagation imaging system with twenty-kilohertz scanning frequency for nondestructive evaluation applications. P of Advances in Structural Health Management and Composite Structures. 2014;1:181-4.
[9] Mascareñas D, Chong SY, Park G, Lee J, Farrar C. Application of compressed sensing to 2-D ultrasonic propagation imaging system data. 6th European Workshop on Structural Health Monitoring2012. p. 1-8.
[10] Di Ianni T, De Marchi L, Perelli A, Marzani A. Compressive sensing of full wave field data for structural health monitoring applications. IEEE transactions on ultrasonics, ferroelectrics, and frequency control. 2015;62:1373-83.

[11] Mesnil O, Ruzzene M. Sparse wavefield reconstruction and source detection using compressed sensing. Ultrasonics. 2016;67:94-104.
[12] Park B, Sohn H, Liu P. Accelerated noncontact laser ultrasonic scanning for damage detection using combined binary search and compressed sensing. Mechanical Systems and Signal Processing. 2017;92:315-33.
[13] Harley JB, Chia CC. Statistical partial wavefield imaging using Lamb wave signals. Structural Health Monitoring. 2017;0:1475921717727160.
[14] Harley JB, Moura JMF. Sparse recovery of the multimodal and dispersive characteristics of Lamb waves. The Journal of the Acoustical Society of America. 2013;133:2732-45.
[15] Remi R, Schnass K. Dictionary Identification - Sparse Matrix-Factorization via L1-Minimization. IEEE Transactions on Information Theory. 2010;56:3523-39.